Check for updates

On the Robustness of the Determination of Metal-Induced Recombination from Photoluminescence Images on Solar Cells

Cyril Leon, Pierre Saint-Cast, Andreas Fell, Johannes M. Greulich,* and Stefan Rein*

The robustness of a recently developed method to obtain the recombination current–density ($J_{0,met}$) under the front metallization fingers of silicon solar cells is investigated. This method requires a voltage-calibrated photoluminescence (PL) imaging setup and can be applied on finished solar cells without any dedicated sample preparation. The Fourier-transform photoluminescence method (FTPL) compares the Fourier spectrum of a PL image with an analytical model to deduce $J_{0,met}$. It is demonstrated here, from sensitivity analysis, repeated measurements, and case studies, that the method allows to differentiate groups of solar cells having undergone different metallization conditions. Moreover, the comparison of the FTPL method with *I–V* measurements and with the area-weighted approach for the $J_{0,met}$ determination shows similar results. Finally, using Quokka modeling, some limitations of the method are identified, and opportunities for improvement are proposed to further enhance this characterization technique.

1. Introduction

Silicon-based solar cells have reached impressive efficiency records during the past years with 25% efficiency for the best passivated emitter and rear cells (PERCs), 26% for the best tunnel oxide passivated contact cells (TOPCon), and even 26.8% for the best heterojunction solar cells (HJT).[1] Even higher efficiency could be reached if progress is made in terms of optimizing the metallization process, which is still responsible for a considerable amount of losses in energy conversion. Therefore, it is important to develop new characterization methods to support innovation in the fabrication field.

A good indicator of the recombination losses at the metal contact is the saturation current–density at the interface between the metal and the emitter of the solar cell ($J_{0,met}$). Several methods already exist to determine this property either by carrying out measurements before and after the metallization steps or using test cells with different metallization patterns.[2–11] Recently, a promising technique based on Fourier-transform photoluminescence imaging (FTPL) has been developed by Saint-Cast et al. with many advantages:[12] 1) the method is nondestructive, 2) it is based on PL imaging, which is a widely used characterization technique[13] and is inline-applicable, 3) it does not require any specific preparation of the sample, which means that it can be applied on finished cells as well as on test samples, and 4) the model on which the FTPL method is based is simple and requires no complex modeling.[12,14] Moreover, we believe that it could even lead to a spatially resolved determination of the metal-induced recombination.

However, the robustness of the method has not yet been sufficiently demonstrated. This article focuses on several crucial aspects of the FTPL technique, exploring the limits of this characterization tool and giving indications on the necessary precautions for best usage.

2. Working Principle

Saint-Cast's FTPL method proposes to extract 1) the implied open-circuit voltage (iV_{OC}), that is, the open-circuit voltage excluding recombination at the metal contacts, and 2) the recombination current density at the metal interface ($J_{0,met}$) from PL images converted into voltage scale. To illustrate the working principle with an example, **Figure 1**a shows the PL image taken from a M2-sized p-type PERC solar cell, calibrated to voltage. Due to the regular distance between the fingers of the front metallization pattern, the voltage profile perpendicular to the grid fingers is periodic, as shown in Figure 1b. Therefore, the signal can be decomposed into a Fourier spectrum, as illustrated on Figure 1c, and the amplitude of the Fourier coefficients can be linked with the iV_{OC} and the $J_{0,met}$ of the cell as developed by Saint-Cast et al.[12,14] With the parameters presented in **Table 1** and assuming a theoretical value for iV_{OC} and V_{max} (the maximum voltage in

C. Leon, P. Saint-Cast, A. Fell, J. M. Greulich, S. Rein
Division Photovoltaics
Fraunhofer Institute for Solar Energy Systems
Heidenhofstr. 2, D-79110 Freiburg, Germany
E-mail: cyril.leon@ise.fraunhofer.de;
johannes.greulich@ise.fraunhofer.de

The ORCID identification number(s) for the author(s) of this article can be found under https://doi.org/10.1002/solr.202300539.

© 2023 The Authors. Solar RRL published by Wiley-VCH GmbH. This is an open access article under the terms of the Creative Commons Attribution-NonCommercial-NoDerivs License, which permits use and distribution in any medium, provided the original work is properly cited, the use is non-commercial and no modifications or adaptations are made.

DOI: 10.1002/solr.202300539

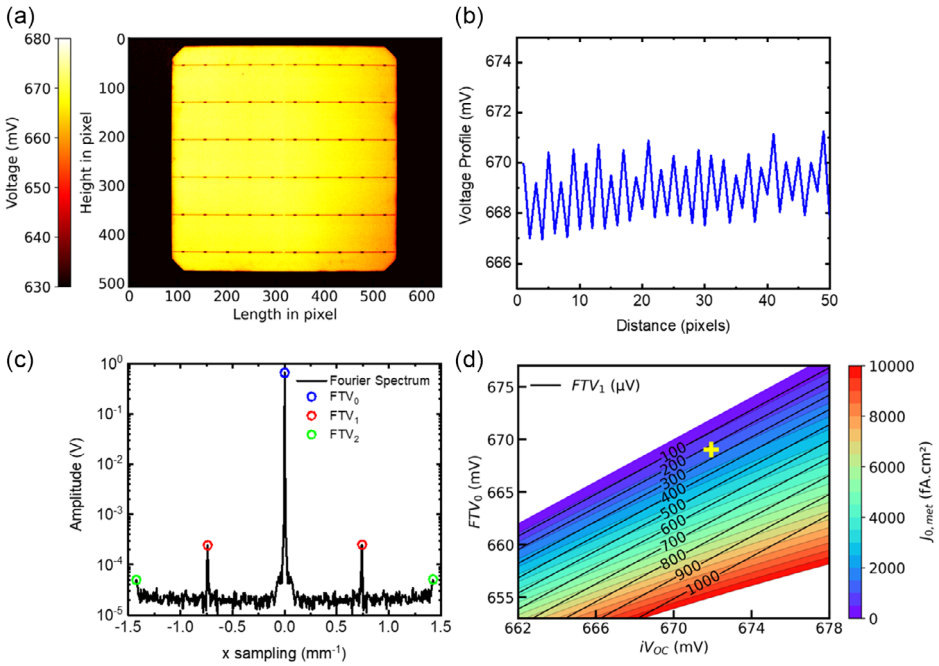

Figure 1. a) Voltage map obtained from the PL image of the studied PERC solar cell, b) horizontal voltage profile extracted from a portion of the PL image, c) amplitude of the corresponding Fourier transform spectrum, d) lookup table calculated using the parameters summarized in Table 1; the yellow cross indicates the intersection point between the measured FTV_0 and FTV_1.

Table 1. Acquisition temperature and sample properties used to calculate the lookup table, where J_{SC} is the short-circuit current density, w is the finger width, and $R_{sq,em}$ and $R_{sq,b}$ are the sheet resistances of the emitter and of the bulk, respectively.

Temperature [K]	$R_{sq,em}$ [Ohm sq^{-1}]	$R_{sq,b}$ [Ohm sq^{-1}]	J_{SC} [mA cm^{-2}]	Pitch [mm]	w [μm]	Thickness [μm]
297.58	88.538	40.188	39.798	1.3478	24	157.56

between two fingers), one can calculate the theoretical values of FTV_0, FTV_1 (the two first Fourier elements) and $J_{0,met}$. However, since iV_{OC} and V_{max} are unknown, they are varied and a lookup table of FTV_0, FTV_1, iV_{OC}, V_{max}, and $J_{0,met}$ is calculated. Figure 1d shows the theoretical values of iV_{OC} (varied) on the x-axis, the theoretical values of FTV_0 (calculated) on the y-axis, while the theoretical values of FTV_1 (calculated) and $J_{0,met}$ (calculated) are represented as contour plots. Once this lookup table is produced, one can report the measured values of FTV_0 and FTV_1 respectively located at $x = 0$ and $x = \pm 1/p$, (p being the pitch) from the Fourier spectrum in the lookup table and deduce the corresponding iV_{OC} and $J_{0,met}$. Based on Figure 1c, one can measure $FTV_0 = 665.8$ mV and $FTV_1 = 245.6$ μV. The intersection of these two values in the lookup table (yellow cross in Figure 1d) allows to deduce $iV_{OC} = 672.3$ mV and $J_{0,met} = 1203.2$ fA cm^{-2}.

3. Relevance and Limitations of the FTPL Method

The analytical model developed by Saint-Cast et al. applies to the case of a relatively simple structure consisting of two laterally homogeneous n- and p-doped layers with metallization fingers located on one side. Finished cells are obviously more complex, with 1) many layers, 2) metallization on both sides of the cell, and 3) different patterns for the front and rear metallization. In this part, results from the FTPL method are confronted to the Quokka model.[15,16]

3.1. Coupling between FTPL Outputs

First, a p–n junction is modeled using Quokka. The n-type emitter and the metallization fingers are located on the front (and illuminated) side. The metallization on the rear side is fully in contact with the semiconductor to allow a homogenous extraction of the charge carriers on this side and ensure that the only source of lateral inhomogeneity comes from the front fingers. The rear recombination is considered negligible and fixed to zero to simulate a structure close to the one described by the Saint-Cast model. On the front, $J_{0,met}$ and $J_{0,pass}$ (the saturation current density at the noncontacted area) are varied and for each parameter variation PL images are modeled in open-circuit condition and analyzed using the FTPL method. The relevant parameters used in modeling are displayed in **Table 2**. The FTPL outputs as function of Quokka inputs are represented in **Figure 2**. One can observe that $J_{0,met}$ obtained from FTPL depends mainly on the

Table 2. Structure settings used in Quokka. ρ_b is the bulk resistivity.

$R_{sq,em}$ [Ohm sq^{-1}]	ρ_b [Ohm.cm]	Front pitch [mm]	w [μm]	Thickness [μm]	Bulk lifetime [ms]
150	1.62	1.3478	24	180	1.086

© 2023 The Authors. Solar RRL published by Wiley-VCH GmbH

2367198x, 2023, 22, Downloaded from https://onlinelibrary.wiley.com/doi/10.1002/solr.202300539 by Fraunhofer Ise Inst. Solar Energy Systems, Wiley Online Library on [11/11/2024]. See the Terms and Conditions (https://onlinelibrary.wiley.com/terms-and-conditions) on Wiley Online Library for rules of use; OA articles are governed by the applicable Creative Commons License

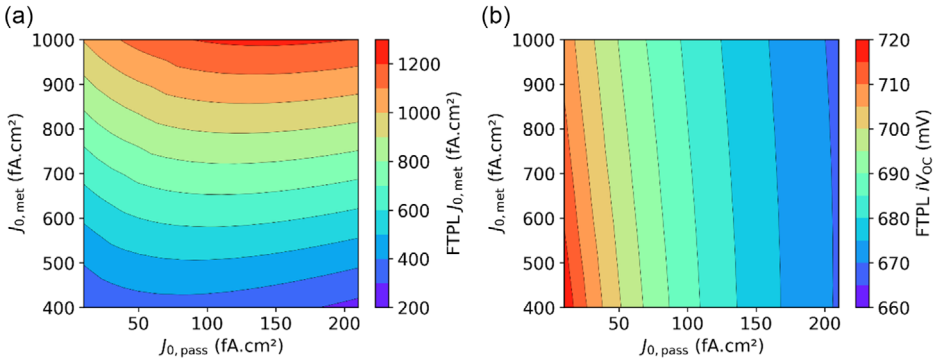

Figure 2. a) $J_{0,met}$ and b) iV_{OC} obtained from FTPL as function of the $J_{0,met}$ and $J_{0,pass}$ used as input in Quokka.

input $J_{0,met}$ as it should be, but it also slightly depends on $J_{0,pass}$ defined in Quokka, especially when the latter is small. On the contrary, the iV_{OC} obtained from FTPL is mostly influenced by $J_{0,pass}$, but it also slightly depends on $J_{0,met}$, especially when $J_{0,pass}$ is small. The two FTPL outputs seem to be coupled; therefore, the interpretation of the FTPL results on experimental studies must be done with caution.

3.2. Impact of the Other Metallization Layer

More complexity is added to modeling by investigating the impact of the rear metallization pattern through three situations: 1) complete rear metallization (but no rear recombination as the reference case), 2) matching pattern, and 3) unmatching pattern (see **Figure 3**). The front pitch is 1.4 mm. For structure B and C, the finger width (50 µm), $J_{0,met}$ (5000 fA cm^{-2}), and $J_{0,pass}$ (50 fA cm^{-2}) are identical for the front and rear sides. For structure B, the rear pitch is equal to the front pitch (1.4 mm), while for structure C, it is equal to 1.0 mm.

Figure 4 shows the voltage profiles simulated with Quokka of these three structures as well as the corresponding Fourier spectra. The voltage variation amplitude being highly related to $J_{0,met}$ extracted from FTPL, it allows to visualize qualitatively how the metallization pattern impacts the FTPL output. When considering the matching pattern situation, the voltage amplitude is almost doubled and so are the harmonics (FTV_1 and FTV_2) in the Fourier spectrum compared to the reference case (note the logarithmic scale in Figure 4b**)**. Both metallization sides

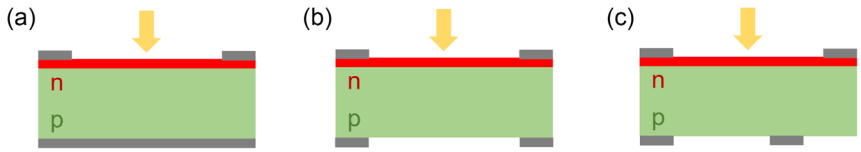

Figure 3. Schematic of the studied structures with a) no rear fingers as the reference structure, b) with matching front and rear pattern, and c) with a different pitch for the rear (1.0 mm) and front (1.4 mm) pattern. The arrow represents the illuminated side.

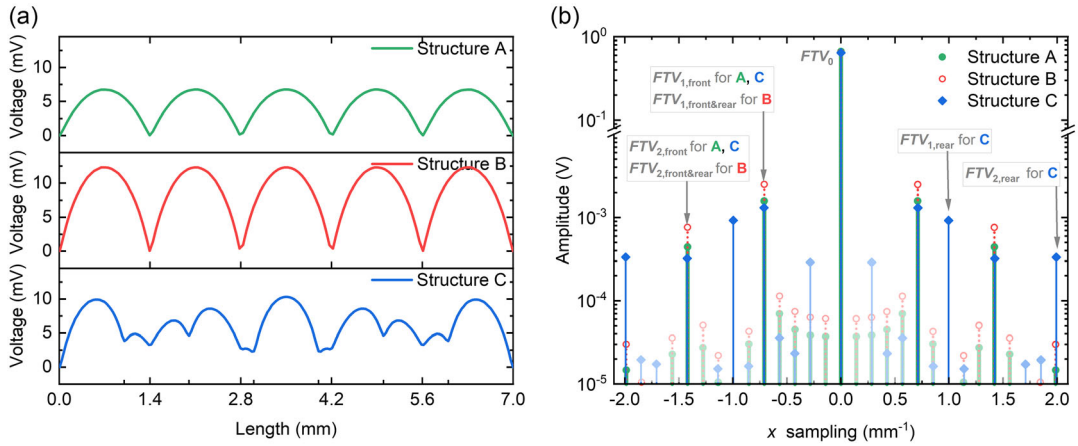

Figure 4. a) Simulated voltage profiles for the different structures represented in Figure 3, b) the amplitudes of their Fourier spectra. Note that the amplitude of the main peak at $x = 0$ and corresponding to the average voltage is also slightly changing from one structure to another. Many peaks related to various other voltage profile symmetries can also be seen but are shaded here for clarity.

© 2023 The Authors. Solar RRL published by Wiley-VCH GmbH

2367198x, 2023, 22, Downloaded from https://onlinelibrary.wiley.com/doi/10.1002/solr.202300539 by Fraunhofer Ise Inst. Solar Energy Systems, Wiley Online Library on [11/11/2024]. See the Terms and Conditions (https://onlinelibrary.wiley.com/terms-and-conditions) on Wiley Online Library for rules of use; OA articles are governed by the applicable Creative Commons License

interfere in a "constructive" way. When the patterns are different, one can observe "constructive" interferences; the more the patterns are in phase and "destructive" interferences, the more the patterns are in phase opposition. In this case, it is possible to observe the front and rear harmonics that are separated in the Fourier spectrum with a slightly lower amplitude than the reference FTV_1. Therefore, as long as the model does not take into account the impact of rear recombination, some errors can be expected. On the other hand, it also shows that the FTPL method could be extended to allow rear-side characterization as well.

3.3. Finger Shading and Setup Influence

The Saint-Cast model describes the voltage profile in between two fingers and does not consider any finger shading. Therefore, in theory, the FTPL method should only be applied on structures with perfectly transparent metallization or simply target areas excluding the fingers. This could be achieved by chopping the PL image in many smaller parts before reconstructing the whole image but without the fingers. This would already be a considerable challenge. But in addition, most PL setups use cameras with a pixel resolution of about a few hundreds of micrometers, which is significantly larger than the finger widths. Therefore, by excluding the pixels shaded by the fingers, a lot of information would be lost. The finger shading combined with the pixel resolution (and other artefacts like blurring, pixel spreading, etc.) contributes to the variation of the PL signal between two fingers that mixes with the impact of the $J_{0,\mathrm{met}}$, making the interpretation of the FTPL outputs even more difficult and the reproduction on different setups more complex. This point will be investigated in more detail in the Experimental Section (Section 5.2).

4. FTPL Accuracy

In addition to the limitations studied in the previous section, several sources of uncertainty may arise when using the method, from the initial parameters required to build the model to the measurement of PL images and their treatment. The main sources of uncertainty are identified and quantified here to determine the accuracy that can be expected from the FTPL method under the best conditions of use.

4.1. Sensitivity Analysis

The input parameters that are used to build the lookup table might not always be known accurately, for example, due to 1) measurement errors of the measured parameters, 2) slight differences between samples within a batch of cells, or 3) spatial inhomogeneities. Thus, understanding their impact on the extracted values of iV_{OC} and $J_{0,\mathrm{met}}$ is important and can give an overview of the achievable accuracy of the method. The influence of each input parameter has been studied one at a time. In addition, we also determined the output variation when all input parameters are varied simultaneously. In order to simulate measurement uncertainties, the input parameters are randomly chosen within Gaussian distributions, assuming realistic max/min values for each parameter around the realistic values already listed in Table 1. The results are represented in **Figure 5**.

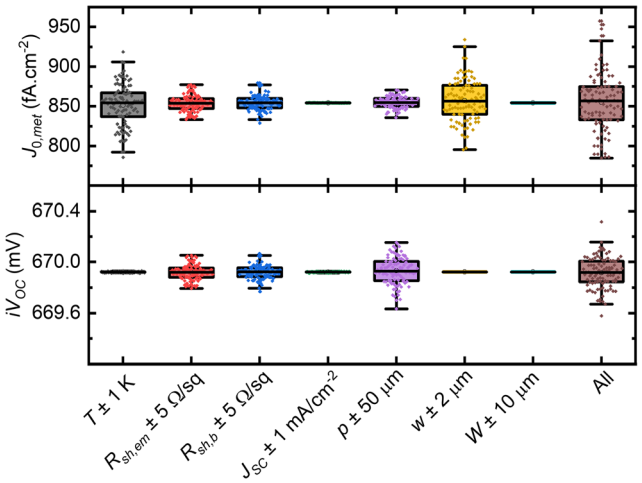

Figure 5. Sensitivity of $J_{0,\mathrm{met}}$ and iV_{OC} with all input parameters randomly varied a) one at a time and b) simultaneously (values labeled "All") within Gaussian distributions with the standard deviations specified on the *x*-axis.

For the considered range of variation of the input parameters, the most critical parameters for an accurate determination of $J_{0,\mathrm{met}}$ are the sample temperature T during the measurement and the finger width w. For future work, it might be important to decrease the impact of these parameters. For a precise iV_{OC}, the sheet resistances $R_{\mathrm{sq,em}}$ and $R_{\mathrm{sq,b}}$ of the layers and the pitch p between two fingers have the most impact, which remain quite low, within a 1 mV range. Thus, precaution must be taken with the input parameters especially for an accurate determination of $J_{0,\mathrm{met}}$.

4.2. Measurements Uncertainties

4.2.1. Reproducibility and Repeatability

Now that uncertainties caused by the parameters building the model have been studied, in the following part, the repeatability and reproducibility of the measurements is verified. For this, several series of PL images are taken on the same PERC sample already studied in the Section 2. For every image, FTV_0 and FTV_1 are extracted from the Fourier spectrum of the PL images in open-circuit condition and iV_{OC} and $J_{0,\mathrm{met}}$ are deduced based on a fixed lookup table calculated from the properties in Table 1. First, the sample is measured 20 times in a row in the exact same position (group A), and then several times with slight changes in the position caused by automatic re-alignment of the cell in our automation system (group B). Finally, those two series of measurements are repeated after a 180° rotation of the sample (group A180 and B180). The FTPL is performed on a wide area covering almost the full cell including busbars. Results are represented in **Figure 6**. For the iV_{OC} values, the method seems quite precise within less than a 0.5 mV range (≈0.1% of error) for every group. For the $J_{0,\mathrm{met}}$ determination, the method is repeatable with deviations of 2% but its reproducibility is less precise with an error up to 15%. The observed relative changes between the groups are due to temperature variation and cell instabilities (probably due to short-term lifetime instabilities in illuminated Ga-doped PERC cells).

© 2023 The Authors. Solar RRL published by Wiley-VCH GmbH

2367198x, 2023, 22, Downloaded from https://onlinelibrary.wiley.com/doi/10.1002/solr.202300539 by Fraunhofer Ise Inst. Solar Energy Systems, Wiley Online Library on [11/11/2024]. See the Terms and Conditions (https://onlinelibrary.wiley.com/terms-and-conditions) on Wiley Online Library for rules of use; OA articles are governed by the applicable Creative Commons License

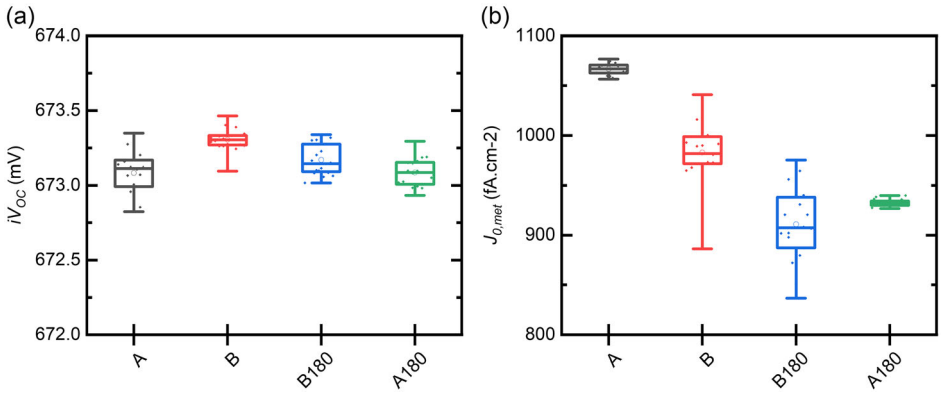

Figure 6. a) iV_{OC} and b) $J_{0,met}$ extracted from PL images for different series of PL measurements with about 20 repeated measurements each. (A) The cell is kept immobile, (B) the position and orientation of the cell slightly changes, (B180) and (A180) same as group B and A but after a 180° rotation of the sample.

4.2.2. Varying the Region of Interest

So far, the FTPL technique has been used over almost the entire cell area. Here, in addition to the full area, five other regions of interest (ROIs) are considered, each between two of the six busbars of the cell. In a first approach, aiming to simulate an area selected by the user, those areas are slightly randomized by a few pixels. Because of some optical artefacts (like vignetting effect[17]) or cell inhomogeneities, the PL counts are lower in areas away from the center. This results in differences in the extracted iV_{OC} (see **Figure 7**). However, the reproducibility of the $J_{0,met}$ is too low to observe the same phenomenon. In fact, a known problem of the fast-Fourier transform (FFT) algorithm that is used in the analysis is that the analyzed signal must be periodic. Otherwise, the Fourier peaks are spread out in frequency with a noisier appearance and increasing uncertainties in the FTV_1 values. Therefore, a second approach was studied, setting the limits of the ROIs with the finger positions to ensure periodic voltage profiles in the selected areas. With this approach, the reproducibility of the FTPL method is highly improved (from ≈±20% to ±2% of $J_{0,met}$ variation) and the impact of the chosen area can now be seen also with the $J_{0,met}$ value allowing spatial determination of the FTPL outputs.

Based on Figure 4, one can conclude that using the FTPL method on a full area gives a $J_{0,met}$ representative of the "average" $J_{0,met}$ of the cell but with poor reproducibility and an underestimated iV_{OC} due to busbars. On the other hand, doing the analysis on an area close to the center of the image, that excludes busbars and matches the finger position, would give more reproducible results less impacted by cell inhomogeneities and optical artefacts. For a relative comparison of different cells, this second approach seems more relevant as long as the same areas are analyzed for every cell.

5. Experimental Usage and Comparison

To determine whether the method can be used to characterize cells that have undergone different metallization conditions, three cases are studied. Here, the FTPL technique is performed on different setups and confronted to other characterization tools: 1) current–voltage (I–V) measurements and 2) the area-weighted approach for the $J_{0,met}$ determination.

5.1. Metallization Paste and Doping Variation

In this first example, 4 groups of around 50 PERC cells whose emitters are doped differently (sheet resistances of 90, 110, 150, and 210 Ohm sq^{-1}) are studied. The samples are screen printed

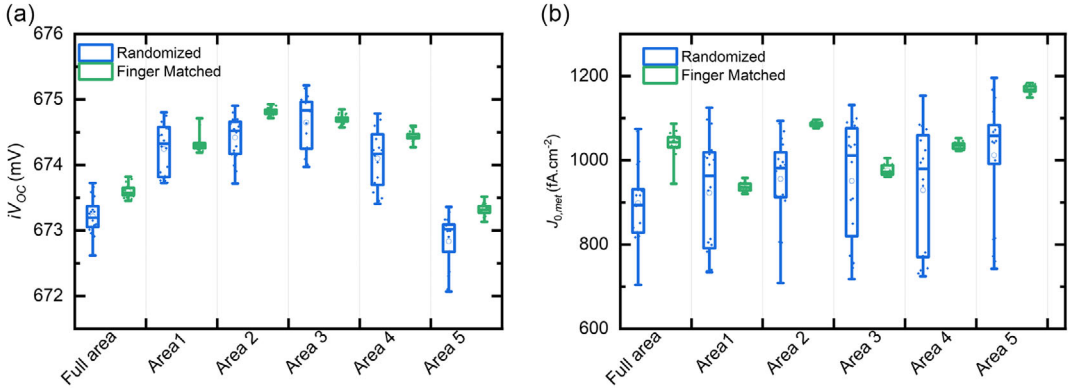

Figure 7. a) iV_{OC} and b) $J_{0,met}$ extracted from PL images measured on the same PERC cells (group B in Section 4.2.1) but for different ROIs. Two approaches are compared: slightly randomizing the ROIs to simulate user selection (blue) and taking an area that matches the fingers periodicity (green).

© 2023 The Authors. Solar RRL published by Wiley-VCH GmbH

2367198x, 2023, 22, Downloaded from https://onlinelibrary.wiley.com/doi/10.1002/solr.202300539 by Fraunhofer Ise Inst. Solar Energy Systems, Wiley Online Library on [11/11/2024]. See the Terms and Conditions (https://onlinelibrary.wiley.com/terms-and-conditions) on Wiley Online Library for rules of use; OA articles are governed by the applicable Creative Commons License

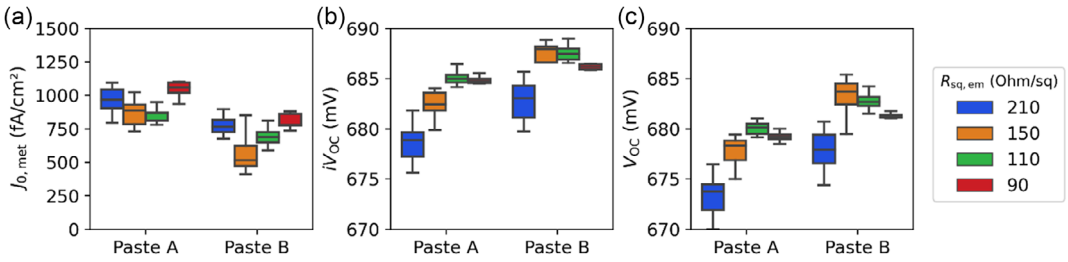

Figure 8. a) $J_{0,met}$ and b) iV_{OC} obtained with the FTPL method on PERC solar cells with different emitter doping and different metallization pastes. c) For comparison, *I–V* measurements are also performed and the V_{OC} is shown here.

with two different pastes (paste A and B) and fired at 820 °C. The cells are characterized using the FTPL method and *I–V* measurements, and results are represented in **Figure 8**. For samples with paste A, the increase of the V_{OC} with the emitter doping density seems to be more related to an increase of the iV_{OC} than to a decrease of the $J_{0,met}$, except for the most-doped samples which show a slightly degraded V_{OC} (compared to the best values) that seems to be correlated with an increase of $J_{0,met}$. The same type of observation can be made with the groups metallized with paste B except that the highest performances are obtained for cells with lower emitter doping densities than for the paste A groups. Overall, the V_{OC} values obtained for the samples metallized with paste B are higher, which is correlated to a $J_{0,met}$ reduction. Surprisingly, the iV_{OC} also seems to be affected by the change in metallization paste. The hypothesis proposed here is that the FTPL method does not completely succeed in decoupling metal-induced recombination from the rest, as already introduced in Section 3. It might be interesting to replace the analytic Saint-Cast model with a lookup table made with the numeric Quokka model when using the FTPL method, to see if the apparent coupling between the two FTPL outputs can be overcome.

5.2. Setup Influence

Here, four groups of p-type PERC cells that have undergone different metallization conditions (pastes and sintering temperatures) have been studied with the FTPL method on two different experimental setups (A and B). Setup A, suitable for offline analysis, is equipped with an iKon-M 934 CCD camera with a pixel resolution of ≈210 µm,[18] similar to the MODULUM tool commercially available at Intego GmbH, Germany. Setup B, suitable for inline analysis, is a system from ISRA Vision GmbH, Germany, based on the Goldeye G1 P-032 SWIR camera with a pixel resolution of ≈340 µm. **Figure 9** compares the $J_{0,met}$ obtained on every group for both setups. As shown, the qualitative trends in Figure 9a,b are very similar, with simply a factor of 2 between the scales of the *y*-axes. As introduced in Section 3, since setup A has a better resolution, the shaded pixels are more impacted by the fingers. Because of this, the voltage variation between two fingers is approximately twice as high with setup A as with setup B which explains the differences of the absolute values of $J_{0,met}$. This artefact, the effect of finger shading combined with the effects of resolution and blur, either needs to be corrected or requires the use of a high-resolution camera to allow reproducibility of the FTPL method on different setups.

5.3. Comparison with the Area-Weighted Approach

In this third case, the FTPL method is confronted with $J_{0,met}$ obtained from area-weighted PL measurements. The latter method requires special sample preparation, where several regions are covered varying the metal/semiconductor fraction which makes it more difficult to implement than the FTPL approach and not applicable for the characterization of finished

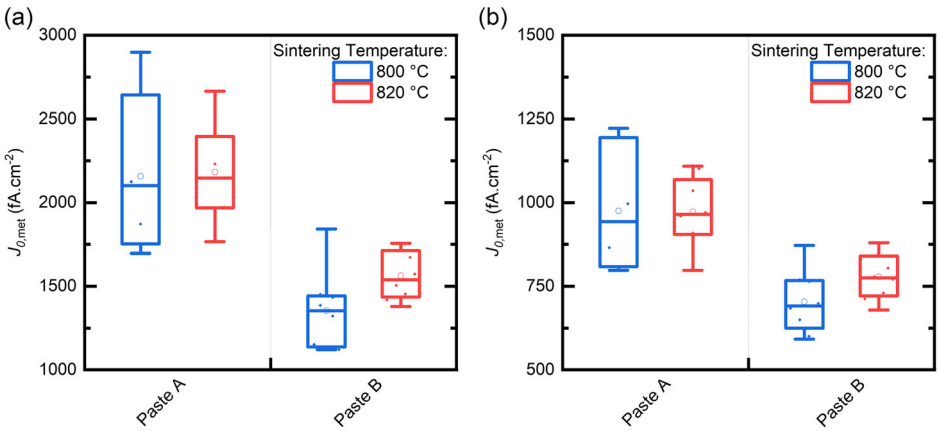

Figure 9. $J_{0,met}$ obtained with the FTPL method on a) PL setup A (210 µm resolution) and b) PL setup B (340 µm resolution). The studied groups of cells vary in terms of the metallization paste and the sintering temperature.

© 2023 The Authors. Solar RRL published by Wiley-VCH GmbH

2367198x, 2023, 22, Downloaded from https://onlinelibrary.wiley.com/doi/10.1002/solr.202300539 by Fraunhofer Ise Inst. Solar Energy Systems, Wiley Online Library on [11/11/2024]. See the Terms and Conditions (https://onlinelibrary.wiley.com/terms-and-conditions) on Wiley Online Library for rules of use; OA articles are governed by the applicable Creative Commons License

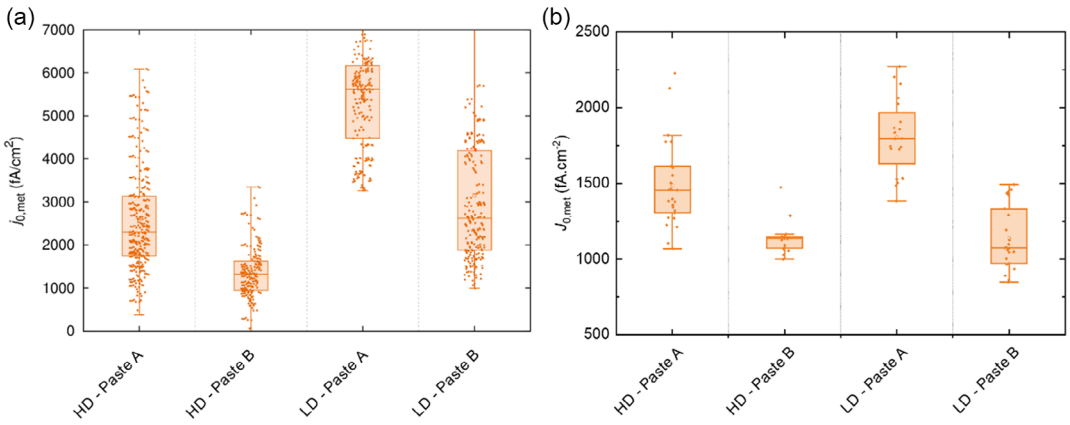

Figure 10. $J_{0,met}$ obtained with a) the area-weighted method and b) the FTPL method applied on PERC solar cells processed with different emitter doping densities (HD for highly doped and LD for lowly doped) as well as with different metallization pastes (A and B).

cells. With the area-weighted approach, the $J_{0,met}$ is extracted from the linear relation between the metallization ratio and the overall saturation current density measured in the targeted area. This is only possible if one assumes a laterally homogeneous p–n junction voltage, neglecting the lateral charge transport while the FTPL method, on the contrary, is based on the analysis of those lateral variations.[8]

Around 20 M2-sized p-type bifacial PERC cells with different emitter doping densities (HD for highly doped and LD for lowly doped) and different metallization pastes (paste A and paste B) are investigated. The samples have been characterized using the two measurements techniques on the two setups described in Section 5.2 (FTPL on the setup B and area-weighted PL on the setup A) and the results are plotted on **Figure 10**. Although the absolute values between the two techniques do not match as it is expected from the use of two different setups, one can observe the same overall behavior: samples with the paste B show higher performances when compared with samples with paste A. However, when comparing samples with different emitters, the variation observed with the area-weighted method is more obvious than with the FTPL method. Since the cells are bifacial

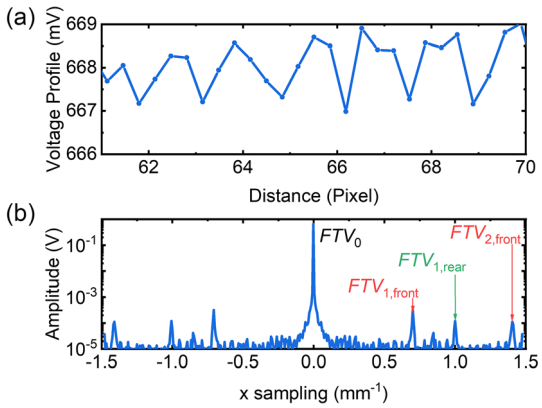

Figure 11. a) Voltage profile measured from calibrated PL measurement on one sample and b) the amplitude of the corresponding Fourier spectrum, the Fourier coefficients related to the front and rear metallization sides being highlighted.

with unmatching pattern (front pitch is 1.4 mm while rear pitch is 1.0 mm), it is however suspected that the FTPL method remains limited by the impact of recombinations on the rear side. However, it is interesting to notice that even with a low-resolution voltage profile (only 4–5 pixels per pitch), the Fourier coefficients related to the rear pattern can still be observed after performing the FTPL analysis (see **Figure 11**). Therefore, by further developing the model to take into account the impact of the rear metallization, the FTPL method could allow to determine the metal-induced recombination on both sides.

6. Conclusion

The FTPL method that determines the $J_{0,met}$ and the iV_{OC} of a finished solar cell from voltage-calibrated PL images is, in a first approach, simple to use and relatively precise. To build the model, particular attention must be given to the measurement of temperature and finger width while a simple estimation of the other sample properties turns out to be sufficient to be able to differentiate between groups that have undergone different metallization conditions. Indeed, an accuracy of 10% can be achieved when the temperature is measured within 1 K and if the fingers width is known within 10% precision. FTPL results are quite sensitive to the analyzed area, especially if the analyzed signal is nonperiodic. Therefore, ROI selection is a crucial step in the analysis and one of the main reasons that limits the reproducibility of the results. When this step is optimized, the method can achieve good reproducibility of the results around 4%.

When the FTPL method is compared with other characterization techniques and Quokka modeling, it appears that the FTPL outputs give relevant information about the recombinations at the contacted (from the $J_{0,met}$) and noncontacted areas (from the iV_{OC}). Indeed, the relative changes, observable via FTPL measurements on samples that have undergone different metallization conditions, are consistent and in agreement with other measured quantities such as the V_{OC} of the cells and the $J_{0,met}$ when measured with the area-weighted approach. However, it appears that the method does not completely decouple metal-induced recombination from the rest. This, combined

© 2023 The Authors. Solar RRL published by Wiley-VCH GmbH

2367198x, 2023, 22, Downloaded from https://onlinelibrary.wiley.com/doi/10.1002/solr.202300539 by Fraunhofer Ise Inst. Solar Energy Systems, Wiley Online Library on [11/11/2024]. See the Terms and Conditions (https://onlinelibrary.wiley.com/terms-and-conditions) on Wiley Online Library for rules of use; OA articles are governed by the applicable Creative Commons License

with several other limiting points (pixel resolution, blurring, finger shading, impact of the rear metallization), complicates the interpretation of the absolute values given by the FTPL method. If the model is extended, the use of Fourier transform could even allow the characterization of metal-induced recombination on both sides of the cell.

For now, the FTPL method is nevertheless a powerful tool for an inline characterization of the front metallization quality, showing good reproducibility.

Acknowledgements

This work was funded by the German Federal Ministry for Economic Affairs and Climate Action within the project "KISS-PV" (03EE1129A).

Open Access funding enabled and organized by Projekt DEAL.

Conflict of Interest

The authors declare no conflict of interest.

Data Availability Statement

The data that support the findings of this study are available from the corresponding author upon reasonable request.

Keywords

characterizations, Fourier analyses, metal-induced recombination, photoluminescence, silicon

Received: July 13, 2023
Revised: August 8, 2023
Published online: September 5, 2023

[1] M. A. Green, E. D. Dunlop, G. Siefer, M. Yoshita, N. Kopidakis, K. Bothe, X. Hao, *Prog. Photovolt: Res. Appl.* **2023**, *31*, 3.
[2] T. Fellmeth, A. Born, A. Kimmerle, F. Clement, D. Biro, R. Preu, *Energy Procedia* **2011**, *8*, 115.
[3] A. Edler, V. D. Mihailetchi, L. J. Koduvelikulathu, C. Comparotto, R. Kopecek, R. Harney, *Prog. Photovolt: Res. Appl.* **2015**, *23*, 620.
[4] V. Shanmugam, T. Mueller, A. G. Aberle, J. Wong, *Sol. Energy* **2015**, *118*, 20.
[5] D. Inns, *Energy Procedia* **2016**, *98*, 23.
[6] R. Dumbrell, M. K. Juhl, T. Trupke, Z. Hameiri, *IEEE J. Photovolt.* **2018**, *8*, 1413.
[7] D. Ananthanarayanan, J. Wong, E.-C. Wang, N. Chen, J. W. Ho, A. G. Aberle, *IEEE J. Photovolt.* **2019**, *9*, 643.
[8] D. Herrmann, S. Lohmuller, H. Hoffler, A. Fell, A. A. Brand, A. Wolf, *IEEE J. Photovolt.* **2019**, *9*, 1759.
[9] M. Li, N. Iqbal, Z. Yang, X. Lin, N. K. Pannaci, C. Avalos, T. Shaw, T. Jurca, K. Davis, *IEEE J. Photovolt.* **2020**, *10*, 1277.
[10] D. Herrmann, D. R. C. Falconi, S. Lohmuller, D. Ourinson, A. Fell, H. Hoffler, A. A. Brand, A. Wolf, *IEEE J. Photovolt.* **2021**, *11*, 174.
[11] S. Guo, S. Johnston, W. V. Schoenfeld, K. O. Davis, in *2018 IEEE 7th World Conf. on Photovoltaic Energy Conversion (WCPEC) (A Joint Conf. of 45th IEEE PVSC, 28th PVSEC & 34th EU PVSEC)*, IEEE, Waikoloa, HI **2018**.
[12] P. Saint-Cast, D. Herrmann, H. Hoffler, *IEEE J. Photovolt.* **2020**, *10*, 554.
[13] T. Trupke, R. A. Bardos, M. C. Schubert, W. Warta, *Appl. Phys. Lett.* **2006**, *89*, 044107.
[14] P. Saint-Cast, A. Fell, *IEEE J. Photovolt.* **2019**, *9*, 1366.
[15] A. Fell, J. Schön, M. C. Schubert, S. W. Glunz, *Sol. Energy Mater Sol. Cells* **2017**, *173*, 128.
[16] A. Fell, *IEEE Trans. Electron Devices* **2013**, *60*, 733.
[17] G. Dost, H. Höffler, J. M. Greulich, *Rev. Sci. Instrum.* **2019**, *90*, 103707.
[18] H. Hannes, F. Schindler, A. Brand, D. Herrmann, R. Eberle, R. Post, A. Kessel, J. Greulich, M. Schubert, in *the 37th European PV Solar Energy Conf. and Exhibition* **2020**.

© 2023 The Authors. Solar RRL published by Wiley-VCH GmbH

2367198x, 2023, 22, Downloaded from https://onlinelibrary.wiley.com/doi/10.1002/solr.202300539 by Fraunhofer Ise Inst. Solar Energy Systems, Wiley Online Library on [11/11/2024]. See the Terms and Conditions (https://onlinelibrary.wiley.com/terms-and-conditions) on Wiley Online Library for rules of use; OA articles are governed by the applicable Creative Commons License